Construction of *n*-body potentials for hcp-bcc metal systems within the framework of embedded atom method

R. F. Zhang, Y. Kong, and B. X. Liu*
Department of Materials Science and Engineering, Tsinghua University, Beijing 100084, China
and National Key Laboratory of Solid-State Microstructure, Nanjing University, Nanjing 210093, China
(Received 8 July 2004; revised manuscript received 29 December 2004; published 9 June 2005)

An effective fitting approach together with *ab initio* calculation is proposed for construction of *n*-body potentials for hcp-bcc metal systems under the framework of the embedded atom method. In two representative systems, i.e., the miscible Co-Nb and immiscible Sc-W systems, the potentials so constructed are proven to be relevant in reproducing some static properties. Moreover, applying the potentials, molecular dynamics simulations using solid solution models predict that the glass-forming ranges of Co-Nb system are within 18–84 at. % of Nb, and reveal that amorphous alloys can be formed with Sc-enriched compositions and the critical solubility of W in the Sc-based solid solution is 15 at. %. Interestingly, the predicted composition ranges favoring metallic glass formation are in good agreement with the experimental observations.

DOI: 10.1103/PhysRevB.71.214102 PACS number(s): 64.70.Kb, 64.70.Pf, 62.20.Dc, 61.50.Ah

I. INTRODUCTION

Atomic-scale simulations based on empirical interatomic potentials of solids/materials have been proven to be useful in understanding some important issues in the field of condensed matter/materials physics and construction of realistic *n*-body potentials is of necessity prior to perform the simulations. In the literature, there have been three major methods together with some modified versions proposed for construction of *n*-body potentials, i.e., the embedded atom method (EAM),[1] the Finnis-Sinclair (FS) model,[2] and the tight-binding (TB) formalism.[3] Generally speaking, the EAM and FS potentials have widely been used for studying the cubic metals,[4,5] whereas the TB potentials have extensively been used for studying the hcp and fcc metals, because of their suitabilities for the metals of respective crystalline structures. Concerning the binary metal systems, there are naturally, three possible combinations among the three major crystalline structures of bcc, fcc, and hcp. To relevantly describe the interactions in the systems, the EAM and TB potentials have frequently been used for the bcc-fcc (e.g., the Cr-Ni system)[6] and hcp-fcc systems (e.g., the Zr-Ni system),[7] respectively, and the remaining hcp-bcc systems have been less studied so far than the bcc-fcc and hcp-fcc systems, though there have been a few examples using EAM potentials to describe the interactions of the pure hcp metals.[5,8,9] In order to develop a complete computational methodology for further modeling and simulation studies, much effort is necessary and should be paid to the hcp-bcc metal systems. The present study is accordingly undertaken and the main objective is (1) to construct *n*-body potentials for some representative hcp-bcc metal systems under the framework of EAM, and (2) to apply the proven realistic *n*-body potentials in molecular dynamics (MD) simulation to study one of the basic issues in the field of metallic glasses, i.e., the glass formation ability/range (GFA/GFR) of the systems.

II. MODEL AND METHOD

In the EAM, the total energy E_{tot}, which can be written as a unique function of the electron density ρ_i, is mainly the energy to embed the atom into the electron density of the neighboring atoms, and supplemented by a short-range doubly screened pair interaction, which accounts for the core-core repulsions.[10] Consequently, the total energy can be expressed by

$$E_{\text{tot}} = \sum_i F_i(\rho_i) + \frac{1}{2}\sum_{i,j(i\neq j)} \phi_{ij}(r_{ij}), \tag{1}$$

where $F(\rho_i)$ is the energy required to embed atom i into the background electron density ρ_i, and $\rho_i = \Sigma_{j\neq i} f_j(r_{ij})$. $f_j(r_{ij})$ is the electron density at the site of atom i contributed by atom j. $\phi_{ij}(r_{ij})$ and r_{ij} are, respectively, the short-range pair potential and the separated distance between atom i and atom j. The electron density function is commonly taken as an exponentially decreasing function,[11] and at a first approximation, the atomic electron density $f(r)$ takes a function form of $f(r) = f_e \exp[-\chi(r/r_e - 1)]$ for both hcp and bcc metals, where f_e is a scaling factor determined by the cohesive energy E_c and the atomic volume Ω. r_e is an equilibrium nearest distance, and χ is an adjustable parameter to be fitted. The embedding function adopts a universal form suggested by Banerjea and Smith[11] and Cai and Ye.[12] Accordingly, the embedding function can be expressed by

$$F(\rho_i) = -F_0\left[1 - \ln\left(\frac{\rho_i}{\rho_e}\right)^n\right]\left(\frac{\rho_i}{\rho_e}\right)^n + F_1\left(\frac{\rho_i}{\rho_e}\right), \tag{2}$$

where $F_0 = E_c - E_v^f$ and E_v^f is the vacancy formation energy. F_1 is an adjustable parameter for the hcp metal and it is set to be zero for the bcc metal. ρ_e is the host electron density at an equilibrium state. According to Banerjea and Smith,[11] a decreasing exponential curvature function combining with the

universal embedding function could yield the model function of Rose *et al.*[13] Consequently, the function proposed by Cai and Ye[12] for the fcc metals is adopted and a little modified for the pair potential $\phi(r)$ of the hcp metals in the present study

$$\phi_{hcp}(r) = -\alpha[1+\beta(r/r_e-1)]\exp[-\beta(r/r_e-1)]. \quad (3)$$

Meanwhile, the function proposed by Johnson and Oh[14] is used for the pair potential of the bcc metals in the present study

$$\phi_{bcc}(r) = \begin{cases} \Phi(r) = k_0 + k_1(r/r_e-1) + k_2(r/r_e-1)^2 + k_3(r/r_e-1)^3, & r_e \leqslant r \leqslant r_s \\ \Phi_a(r) = \Phi(r) + k_a[\Phi(r) - \Phi(r_e)](r/r_e-1)^2, & r < r_e, \end{cases} \quad (4)$$

where r is the interatomic distance, r_e is an equilibrium first-neighbor distance, k_a is a constant in the form of $k_a = 4.5[1+4/(A_r-0.1)]$ depending on an anisotropy ratio A_r, and the cutoff distance (from r_s to r_c) is set to be between the second- and third-neighbor distances.[15] In construction of n-body potentials for the pure hcp metals, the present authors propose the following fitting approach, i.e., using the average bulk and shear moduli, instead of five independent linear elastic constants, together with the cohesive energy, vacancy formation energy and equilibrium lattice constants to fit the potential parameters, and after fitting, five independent linear elastic constants are reproduced by the fitted potentials, thus confirming the relevance of the fitting as well as the parameters. It turns out that the proposed fitting approach is fairly effective, though, in principle, it is also possible to use five independent linear elastic constants in fitting the potential parameters.

The hcp-bcc cross potential takes a simplified form, which was recently proposed for the fcc-bcc metal systems by Gong *et al.*,[16] to combine the hcp-hcp and bcc-bcc potentials

$$\phi_{hcp\text{-}bcc}(r) = A[\phi_{hcp}(r+B) + \phi_{bcc}(r+C)], \quad (5)$$

where A, B, and C are three potential parameters to be fitted.

III. MOLECULAR DYNAMICS SIMULATION

Two representative systems, i.e., the Co-Nb and Sc-W systems, which are characterized by a negative (-37 kJ/mol) and a positive formation enthalpy ($+14$ kJ/mol),[17,18] respectively, are selected in the present study to demonstrate the feasibility of the proposed fitting approach in construction of n-body potentials and the relevance/applicability of the potentials in reproducing the static as well as the dynamic properties of the hcp-bcc metal systems through MD simulations.

A. Construction of *n*-body potential and simulation of the Co-Nb system

For the Co-Nb system, the experimental data of the cohesive energy and elastic constants of the equilibrium Co-Nb compounds are not accessible, and the complexity and uncertainty of the crystalline structures of the equilibrium Co-Nb compounds also constrain the use of these properties in fitting the cross potential.[18,19] For the Sc-W system, there is not even an equilibrium compound and therefore no physical property could be used for fitting the cross potential. In this regard, there have been some reports[20,21] showing that the first-principles calculations are of significant help in acquiring some useful physical properties of the alloy phases necessary for deriving n-body potentials. Accordingly, applying the Vienna *ab initio* simulation package,[22] the total energies and the lattice constants of the two possible $Co_{75}Nb_{25}$ and $Co_{50}Nb_{50}$ nonequilibrium compounds with $L1_2$ and $B2$ structures, respectively, are first calculated and then used in deriving the n-body potential of the Co-Nb system. Concerning the details of the calculations and the fitting procedure, the readers are referred to the recent publication from

TABLE I. Fitted parameters for the Co-Co, Nb-Nb, and Co-Nb potentials.

Co-Co		Nb-Nb		Co-Nb	
χ	7.659 19	χ	10.403 652	A	1.677 400
α(eV)	0.291 56	k_0(eV)	−0.393 145		
β	3.341 78	k_1(eV)	−0.642 187	B(Å)	−0.682 548
r_a(Å)	2.496 84	k_2(eV)	3.593 435		
F_1(eV)	0.447 19	k_3(eV)	−3.787 160	C(Å)	1.117 879
r_s(Å)	3.6	r_s(Å)	3.4		
r_c(Å)	4.4	r_c(Å)	4.4		
n	0.825 17	n	0.440 653		

TABLE II. Comparison between calculated and experimental/*ab initio* values of cohesive energy E_c, lattice constant a and c, average bulk moduli B, average shear moduli G, vacancy formation energy E_v^f, and structure stability (see Refs. 23–25).

		E_c(eV/atom)	a(Å)	c(Å)	B(Mbar)	G(Mbar)	E_v^f(eV)
Co	Experimental	4.39	2.507	4.069	1.948	0.9115	1.46
	This work	4.39	2.507	4.069	1.948	0.9115	1.46
Nb	Experimental	7.47	3.301		1.730	0.4250	2.75
	This work	7.47	3.301		1.730	0.4250	2.75
$Co_{75}Nb_{25}$	*Ab initio*	5.472 43	3.64				
($L1_2$)	Fitted	5.489 08	3.60				
$Co_{50}Nb_{50}$	*Ab initio*	6.016 72	3.07				
($B2$)	Fitted	6.077 79	3.00				

Structure stability

		$E_{bcc}-E_{fcc}$(eV/atom)	$E_{hcp}-E_{fcc}$(eV/atom)	Reference
Co	*Ab initio*	0.0852	−0.0231	
	Hu *et al.*	0.0164	−0.0062	5
	Fitted	0.0356	−0.0029	
Nb	*Ab initio*	−0.3334	−0.0319	
	Johnson *et al.*	−0.27	0	14
	Fitted	−0.2812	0	

authors' group.[16] After the fitting and optimization, the potential parameters are obtained and Table I lists the fitted parameters for the Co-Co, Nb-Nb, and Co-Nb potentials, respectively. Table II and Table III list the comparison between some physical properties reproduced by the constructed potentials and from the experimental/*ab initio* calculated values used initially for fitting the potentials.[23–25] Evidently, the constructed potentials of the Co-Nb system work reasonably well in terms of reproducing some physical properties of the pure Co and Nb as well as those of the possible $Co_{75}Nb_{25}$ and $Co_{50}Nb_{50}$ nonequilibrium compounds. It should be noted that the elastic constants of both pure metals and compounds are necessary to be acquired for testing the many-body potentials. Accordingly, the comparison between the calculated and experimental /*ab initio* values of independent second-order elastic constants of hcp-Co, bcc-Nb, $L1_2$-Co_3Nb, and $B2$-CoNb are listed separately in Table III. From the table, it can clearly be observed that the independent second-order elastic constants for both pure metals and compounds can indeed be reproduced reasonably. In addition, the energy differences between the three major crystalline structures for pure metals Co and Nb are also calculated by the present potentials, by Johnson and Hu's potentials and obtained by *ab initio* calculation, and are listed in Table II. Take the energy difference between the bcc and fcc Nb as an example, one can see from the table that the presently calculated value $E_{bcc}-E_{fcc}=-0.2812$ eV/atom is quite comparable with $E_{bcc}-E_{fcc}=-0.27$ eV/atom calculated by Johnson's potential, and is smaller than $E_{bcc}-E_{fcc}=-0.3334$ eV/atom obtained by *ab initio* calculation. Apparently, all the calculated results confirm that the most stable structure of Nb is of bcc. It is also true for the Co that all the calculated results confirm the most stable structure is hcp. Experimentally, an intermediate $L1_2$-$Co_{75}Nb_{25}$ phase has been obtained and its lattice constant was determined to be 3.66 Å,[26] which is consistent with the results of 3.60 and 3.64 Å deduced from the present

TABLE III. Comparison between the calculated and experimental /*ab initio* values of independent second-order elastic constants of hcp-Co, bcc-Nb, $L1_2$-Co_3Nb, and $B2$-CoNb (see Ref. 25).

		C_{11}(Mbar)	C_{12}(Mbar)	C_{13}(Mbar)	C_{33}(Mbar)	C_{44}(Mbar)
Co	Experimental	3.195	1.661	1.021	3.736	0.824
	This work	3.275	1.350	1.178	3.569	0.728
Nb	Experimental	2.5270	1.3320			0.3097
	This work	2.5270	1.3320			0.3097
$L1_2$-Co_3Nb	*Ab initio*	3.6834	1.6395			1.5996
	This work	3.1614	1.9878			1.3774
$B2$-CoNb	*Ab initio*	2.5094	1.7299			0.6044
	This work	2.3931	1.7280			0.2374

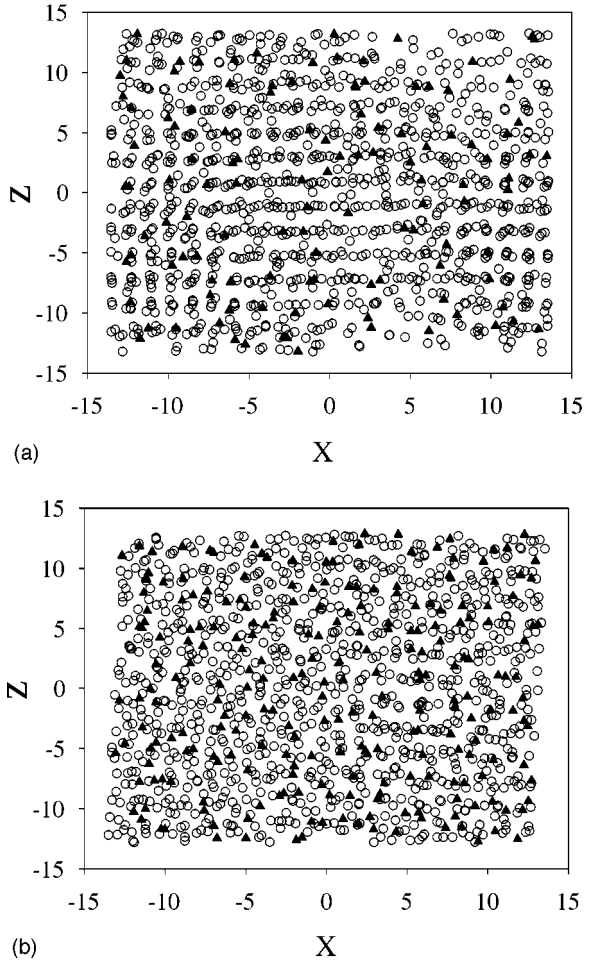

FIG. 1. The projections of atomic positions of (a) $Co_{90}Nb_{10}$, and (b) $Co_{80}Nb_{20}$ hcp-solid solution models, respectively, after annealing at 300 K for 2 ns. Open circles: Co. Filled triangles: Nb.

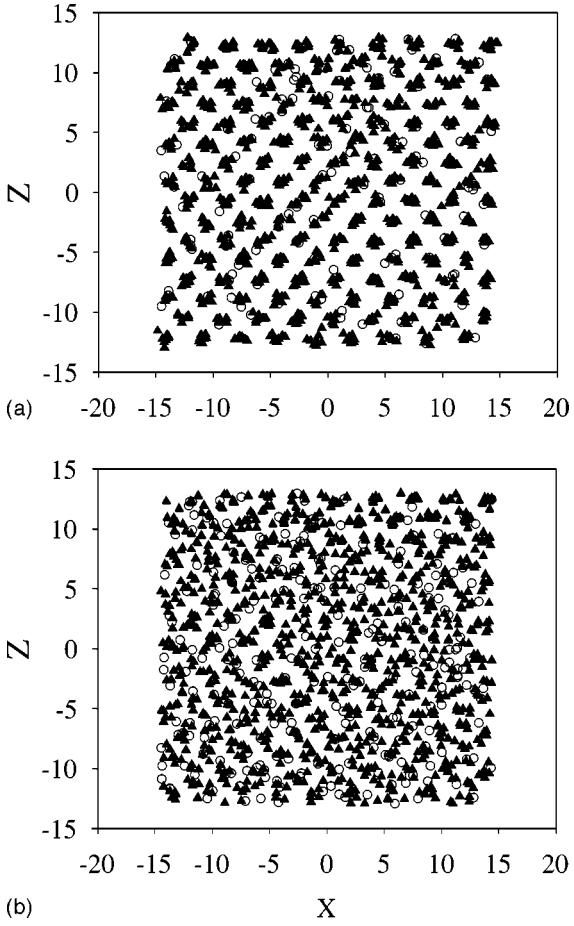

FIG. 2. The projections of atomic positions of (a) $Co_{10}Nb_{90}$, and (b) $Co_{20}Nb_{80}$ bcc-solid solution models, respectively, after annealing at 300 K for 2 ns. Open circles: Co. Filled triangles: Nb.

n-body potential and obtained by *ab initio* calculation, respectively. Obviously, all the above results lend further support to the relevance of the newly constructed potentials.

The fitted potentials should also reproduce dynamic properties of the materials studies. Here we have also performed some important tests. For example, employing the constructed potentials for Co and Nb, the melting points of pure Co and Nb were determined by means of MD simulations to be about 1910 and 2850 K, respectively, which are in reasonably good agreement with the mean experimental values (i.e., 1768 K for Co and 2741 K for Nb, respectively). It can therefore be considered that the constructed Co-Nb potentials are capable of describing the atomic interaction expediently even when inharmonic effects play a major role for the two metals.

Employing the constructed Co-Nb potentials, MD simulations using the hcp and bcc solid solution models are carried out, respectively, to study the crystal-to-amorphous transition in the Co-Nb system. Concerning the details of the MD scheme and the structural characterization methods, the readers are referred to recent publication from author's group.[27] As it has been shown that the GFR of a binary metal system is the composition range bounded by the two terminal critical solid solubilities, below which the solid solution would retain its crystalline state, while beyond which the solid solution would transform into a disordered/amorphous state.[28] Accordingly, in the hcp solid solution model, the amount of

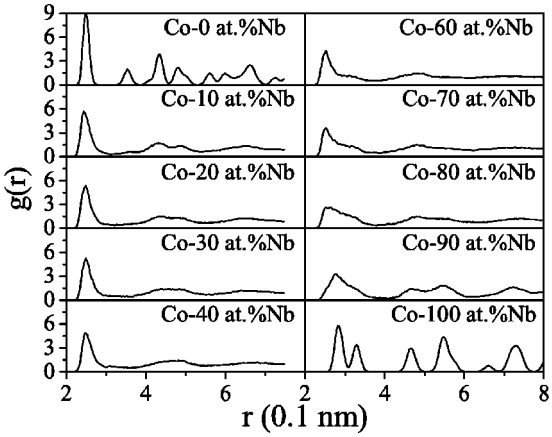

FIG. 3. For the Co-Nb system, the calculated total pair correlation functions of the solid solution models upon annealing at 300 K for 2 ns. (Note: the left five lines are for the hcp solid solution models and the right five lines are for the bcc solid solution models.)

TABLE IV. Fitted parameters for the Sc-Sc, W-W, and Sc-W potentials.

Sc-Sc		W-W		Sc-W	
χ	6.417 256	χ	6.155 980	A	1.108 85
α(eV)	0.311 282	k_0(eV)	−0.547 671		
β	1.226 141	k_1(eV)	−2.130 315	B(Å)	0.698 26
r_a(Å)	2.662 559	k_2(eV)	16.808 946		
F_1(eV)	0.712 605	k_3(eV)	−8.503 413	C(Å)	0.307 02
r_s(Å)	3.4	r_s(Å)	3.2		
r_c(Å)	4.4	r_c(Å)	4.4		
n	1.25	n	0.44		

Nb solute atoms is gradually increased until reaching a critical value, at and beyond which the solid solution becomes energetically unstable and collapses into a disordered state, thus determining the critical solid solubility of Nb in Co. Similar simulations are also performed to determine the critical solid solubility of Co in Nb. As a typical example to show the determination of the critical solid solubility of the Co-Nb system, Figs. 1 and 2 exhibit the projections of atomic positions of the $Co_{90}Nb_{10}$, $Co_{80}Nb_{20}$, $Co_{20}Nb_{80}$, and $Co_{10}Nb_{90}$ solid solution models after annealing at 300 K for 2 ns, respectively. It can be seen vividly that a uniform disordered structure is formed in the $Co_{80}Nb_{20}$ and $Co_{20}Nb_{80}$ solid solution models, while the $Co_{90}Nb_{10}$ and $Co_{10}Nb_{90}$ solid solution models still remain in a partially ordered state, indicating that the critical solid solubility to trigger the crystal-to-amorphous transition is between 10 and 20 at. % of Nb for the Co-rich side and 80 and 90 at. % of Nb for the Nb-rich side, respectively. Besides, it is recognized that the total pair correlation functions are considered as a decisive measure to confirm a disordered state. Figure 3 exhibits the calculated total pair correlation functions of the Co-based hcp and Nb-based bcc solid solution models upon annealing at 300 K for 2 ns. In Fig. 3, the left five lines are for the hcp solid solution models and the right five lines are for the bcc solid solution models. One sees clearly that in the Co-rich side, beyond 20 at. % of Nb, the hcp solid solutions have transformed into amorphous states, and that in the Nb-rich side, beyond 80 at. % of Nb, the bcc solid solutions remain in crystalline states. We further study in detail the two composition ranges, i.e., within 10–20 at. % of Nb and within 80–90 at. % of Nb, respectively, and the simulations determine the two critical solid solubilities of the Co-Nb system are 18 at. % of Nb in Co and 16 at. % of Co in Nb, respectively. Consequently, the GFR of the Co-Nb system determined directly from the interatomic Co-Nb potential through MD simulations is within 18–84 at. % of Nb, which is in excellent agreement with the experimental observations (i.e., 20–80 at. % of Nb) reported in the literature.[29,30]

TABLE V. Comparison between the calculated and experimental/*ab initio* values of cohesive energy E_c, lattice constant a and c, average bulk moduli B, average shear moduli G, vacancy formation energy E_v^f, and structure stability (see Refs. 23–25).

		E_c(eV/atom)	a(Å)	c(Å)	B(Mbar)	G(Mbar)	E_v^f(eV)
Sc	Experimental	3.90	3.308	5.267	0.558	0.3067	1.15
	This work	3.90	3.308	5.267	0.558	0.3067	1.15
W	Experimental	8.66	3.165		3.1029	1.599	3.95
	This work	8.66	3.165		3.1029	1.599	3.95
$Sc_{75}W_{25}$	*Ab initio*	4.9244	4.34				
($L1_2$)	Fitted	4.9471	4.28				
$Sc_{50}W_{50}$	*Ab initio*	5.8245	3.31				
($B2$)	Fitted	5.9148	3.39				

		Structure stability		
		$E_{bcc}-E_{fcc}$(eV/atom)	$E_{hcp}-E_{fcc}$(eV/atom)	Reference
Sc	*Ab initio*	0.1084	−0.0409	
	Hu *et al.*	0.0501	−0.0010	5
	Fitted	0.0261	−0.0001	
W	*Ab initio*	−0.4585	0.0187	
	Johnson *et al.*	−0.07	0	14
	Fitted	−0.0295	0	

TABLE VI. Comparison between the calculated and experimental/*ab initio* values of independent second-order elastic constants of hcp-Sc, bcc-W, $L1_2$-Sc_3W, and *B*2-ScW (see Ref. 25).

		C_{11}(Mbar)	C_{12}(Mbar)	C_{13}(Mbar)	C_{33}(Mbar)	C_{44}(Mbar)
hcp-Sc	Experimental	0.9926	0.3968	0.2932	1.0701	0.2723
	This work	0.9359	0.3436	0.3324	1.1326	0.2859
bcc-W	Experimental	5.2239	2.0453			1.6072
	This work	5.2239	2.0453			1.6072
$L1_2$-Sc_3W	*Ab initio*	1.1785	0.7126			0.5536
	This work	1.2616	0.9780			0.4642
*B*2-ScW	*Ab initio*	1.0184	1.5630			0.4643
	This work	2.3483	2.1033			0.4899

B. Construction of *n*-body potential and simulation of the Sc-W system

Similar *ab initio* calculations and potential fitting are also conducted for another representative hcp-bcc metal system, i.e., the immiscible Sc-W system with a positive heat of enthalpy, and an *n*-body Sc-W potential is thus constructed. Table IV lists the fitted parameters for the Sc-Sc, W-W, and Sc-W potentials, respectively. Table V list the comparison between some physical properties reproduced by the constructed potentials and from the experimental/*ab initio* calculated values used initially for fitting the potentials[23–25] and Table VI lists the comparison between the calculated and experimental/*ab initio* values of independent second-order elastic constants of hcp-Sc, bcc-W, $L1_2$-Sc_3W, and *B2*-ScW, respectively. Evidently, the constructed potentials of the Sc-W system also work reasonably well in terms of reproducing some physical properties of the pure Sc and W, as well as those of the possible $Sc_{75}W_{25}$ and $Sc_{50}W_{50}$ nonequilibrium compounds in the system. One may note from the values listed in Table VI that the independent second-order elastic constants C_{11} and C_{12} of *B2*-ScW determined by the present potential is about two times higher than that obtained from *ab initio* calculations, which, to the author's view, may generally be acceptable for an empirical many-body potential. In addition, the energy differences between the three major crystalline structures for pure metals Sc and W are also calculated by the present potentials, by Johnson and Hu's potentials and obtained by *ab initio* calculation, and are listed in Table V. Take the energy difference between bcc and fcc W as an example, one sees from the table that the

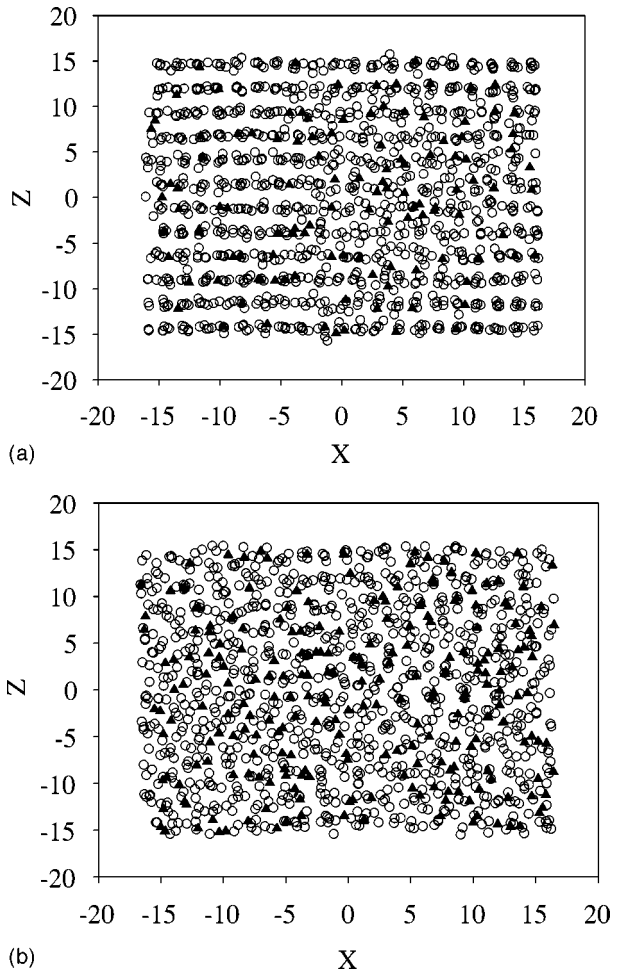

FIG. 4. The projections of atomic positions of (a) $Sc_{90}W_{10}$, and (b) $Sc_{80}W_{20}$ solid solution models, respectively, after annealing at 300 K for 2 ns. Open circles: Sc. Filled triangles: W.

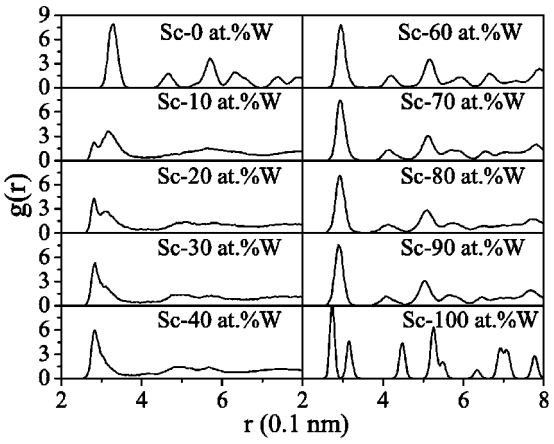

FIG. 5. For the Sc-W system, the calculated total pair correlation functions of the solid solution models upon annealing at 300 K for 2 ns. (Note: the left five lines are for the hcp solid solution models and the right five lines are for the bcc solid solution models.)

presently calculated value $E_{bcc}-E_{fcc}=-0.0295$ eV/atom is comparable with $E_{bcc}-E_{fcc}=-0.07$ eV/atom obtained from Johnson's, and is smaller than $E_{bcc}-E_{fcc}=-0.4585$ eV/atom obtained by *ab initio* calculation. One may also note that the values of $E_{fcc}-E_{hcp}$ of Sc determined by the present potential (0.0001 eV/atom) and by Hu's potential (0.001 eV/atom) is about 40 and 4 times, respectively, lower than that obtained from *ab initio* calculations. In this regard, such kind of discrepancy has been frequently observed, as one could not expect that the empirical many-body potentials could reproduce all the related properties precisely. Nonetheless, the above result, at least, correctly suggests that the hcp structure is energetically lower than the fcc structure for Sc. Similarly, it is also true for W that the most stable structure is of bcc. These results could serve as convincing evidence confirming the relevance of the newly constructed potentials.

Before employing the constructed Sc-W potentials to perform the MD simulation for studying the GFR of the Sc-W system, the melting points of pure metals Sc and W are estimated to be about 2020 and 3850 K, respectively, which are in reasonably good agreement with the mean experimental values (1812 K for Sc and 3680 K for W, respectively). It can therefore be considered that the constructed Sc-W potentials are capable of describing the atomic interaction expediently even when inharmonic effects play a major role for the two metals. The constructed Sc-W potentials are then applied to perform MD simulations to determine the GFR of the Sc-W system. As a typical example to show the determination of the critical solid solubility of W in Sc, Fig. 4 exhibits the projections of atomic positions of the $Sc_{90}W_{10}$ and $Sc_{80}W_{20}$ solid solution models after annealing at 300 K for 2 ns, respectively. It can be seen vividly that a uniform disordered structure is formed in the $Sc_{80}W_{20}$ solid solution model, while the $Sc_{90}W_{10}$ solid solution model still remains in an ordered state, indicating that the critical solid solubility to trigger the crystal-to-amorphous transition is between 10 and 20 at. % of W. Figure 5 exhibits the calculated total pair correlation functions of the Sc-based hcp and W-based bcc solid solution models, respectively, upon annealing at 300 K for 2 ns. One sees clearly that in the Sc-rich side, beyond 10 at. % of W, the hcp solid solutions have transformed into amorphous states, and that in the W-rich side, the bcc solid solutions remain in crystalline states. We further study in detail the composition range of 10–20 at. % of W and determine that the critical solid solubility of W in Sc is 15 at. %. It is therefore deduced that amorphous alloys can readily be formed in the Sc-rich side, whereas in the W-rich side, amorphous alloy can hardly be obtained. In order to validate the prediction, we performed ion beam mixing experiments using Sc-W multilayered samples with various overall alloy compositions. Interestingly, in the Sc-rich side, two amorphous alloys were indeed obtained in the $Sc_{75}W_{25}$ and $Sc_{60}W_{40}$ multilayered samples upon 200 keV xenon ion irradiation to a dose of $9\times10^{15}Xe^{+}/cm^{2}$, whereas in the W-rich side, unique amorphous phase was not observed in the $Sc_{25}W_{75}$ and $Sc_{40}W_{60}$ multilayered samples upon irradiation up to the highest dose of $1\times10^{16}Xe^{+}/cm^{2}$ conducted in the present study. Apparently, these experimental results are in support with the above simulation results.

IV. CONCLUSION

In summary, we have developed an effective fitting approach for construction of *n*-body potentials of the hcp-bcc metal systems under the framework of embedded atom method. The constructed *n*-body potentials are proven to be relevant in reproducing the static properties and some dynamic properties of the systems as well as in determining the composition ranges favoring the formation of amorphous alloys of the systems through molecular dynamics simulations.

ACKNOWLEDGMENTS

The authors are grateful for the financial support from the National Natural Science Foundation of China, The Ministry of Science and Technology of China (through Grant No. G20000627-07), and the Administration of Tsinghua University.

*Author to whom correspondence should be addressed. E-mail: dmslbx@tsinghua.edu.cn

[1] M. S. Daw and M. I. Baskes, Phys. Rev. Lett. **50**, 1285 (1983).
[2] M. W. Finnis and J. E. Sinclair, Philos. Mag. A **50**, 45 (1984).
[3] D. Tomanek, S. Mukherjee, and K. H. Bennemann, Phys. Rev. B **28**, 665 (1983).
[4] D. J. Bacon, J. Nucl. Mater. **159**, 176 (1988).
[5] W. Y. Hu, B. W. Zhang, B. Y. Huang, F. Gao, and D. J. Bacon, J. Phys.: Condens. Matter **13**, 1193 (2001).
[6] J. K. Chen, D. Farkas, and W. T. Reynolds, Jr., Acta Mater. **45**, 4415 (1997).
[7] C. Massobrio, V. Pontikis, and G. Martin, Phys. Rev. B **41**, 10486 (1990).
[8] D. J. Oh and R. A. Johnson, J. Mater. Res. **3**, 471 (1988).
[9] M. I. Baskes and R. A. Johnson, Modell. Simul. Mater. Sci. Eng. **2**, 147 (1994).
[10] S. M. Foiles, Phys. Rev. B **32**, 3409 (1985).
[11] A. Banerjea and J. R. Smith, Phys. Rev. B **37**, 6632 (1988).
[12] J. Cai and Y. Y. Ye, Phys. Rev. B **54**, 8398 (1996).
[13] J. H. Rose, J. R. Smith, F. Guinea, and J. Ferrante, Phys. Rev. B **29**, 2963 (1984).
[14] R. A. Johnson and D. J. Oh, J. Mater. Res. **4**, 1195 (1989).
[15] A. M. Guellil and J. B. Adams, J. Mater. Res. **7**, 639 (1992).
[16] H. R. Gong, L. T. Kong, W. S. Lai, and B. X. Liu, Phys. Rev. B **66**, 104204 (2002).
[17] R. F. Zhang and B. X. Liu, Appl. Phys. Lett. **81**, 1219 (2002).
[18] F. R. deBoer, R. Boom, W. C. M. Mattens, A. R. Miedema, and A. K. Niessen, *Cohesion in Metals: Transition Metal Alloys* (North Holland, Amsterdam, 1989).
[19] T. B. Massalski, *Binary Alloy Phase Diagrams* (ASM International, Materials Park, OH, 1990).
[20] D. E. Luzzi, M. Yan, M. Sob, and V. Vitek, Phys. Rev. Lett. **67**,

1894 (1991).
[21] M. Yan, M. Sob, D. E. Luzzi, V. Vitek, G. J. Ackland, M. Methfessel, and C. O. Rodriguez, Phys. Rev. B **47**, 5571 (1993).
[22] G. Kresse and J. Hafner, Phys. Rev. B **47**, 558 (1993).
[23] C. Kittel, *Introduction to Solid-State Physics* (Wiley, New York, 1976).
[24] E. A. Brandes and G. B. Brook, *Smithells Metals Reference Book*, 7th ed. (Butterworth-Heinemann, Oxford, 1992).
[25] G. Simmons and H. Wang, *Single Crystal Elastic Constants and Calculated Aggregate Properties: A Handbook*, 2nd ed. (MIT Press, Cambridge, 1971).
[26] V. V. Kokorin and K. V. Chuistov, Fiz. Met. Metalloved. **26**, 375 (1968).
[27] W. S. Lai and B. X. Liu, Phys. Rev. B **58**, 6063 (1998).
[28] B. X. Liu, W. S. Lai, and Q. Zhang, Mater. Sci. Eng., R. **244**, 1 (2000).
[29] Z. J. Zhang and B. X. Liu, J. Phys.: Condens. Matter **6**, 2647 (1994).
[30] J. Gfeller, A. Blatter, and U. Kambli, J. Less-Common Met. **145**, 105 (1988).